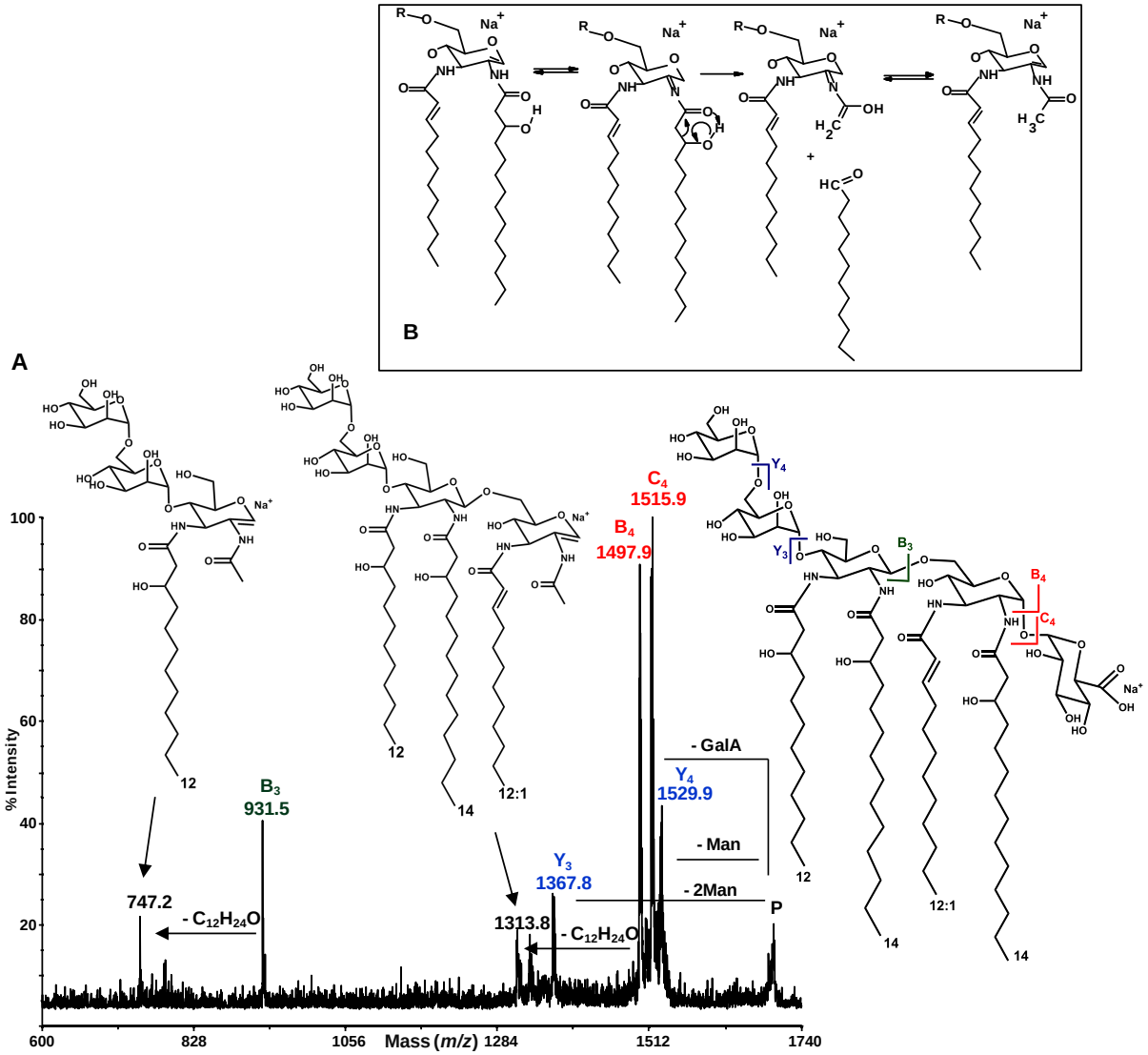

Supplementary Figure 1: MS^2 of *O*-deacylated lipid A.

a. MALDI TOF/TOF MS^2 analysis of the *O*-deacylated lipid A from *Bradyrhizobium*BTAi1, whose structure has been also sketched. (GalA, Galacturonic acid; Man, Mannose)

b. Losses of $C_{12}H_{24}O$ from B ions refer to a six point molecular rearrangement involving the free 3-OH group on the 14:0 acyl chains. P: parent ion at *m/z* 1691.76.

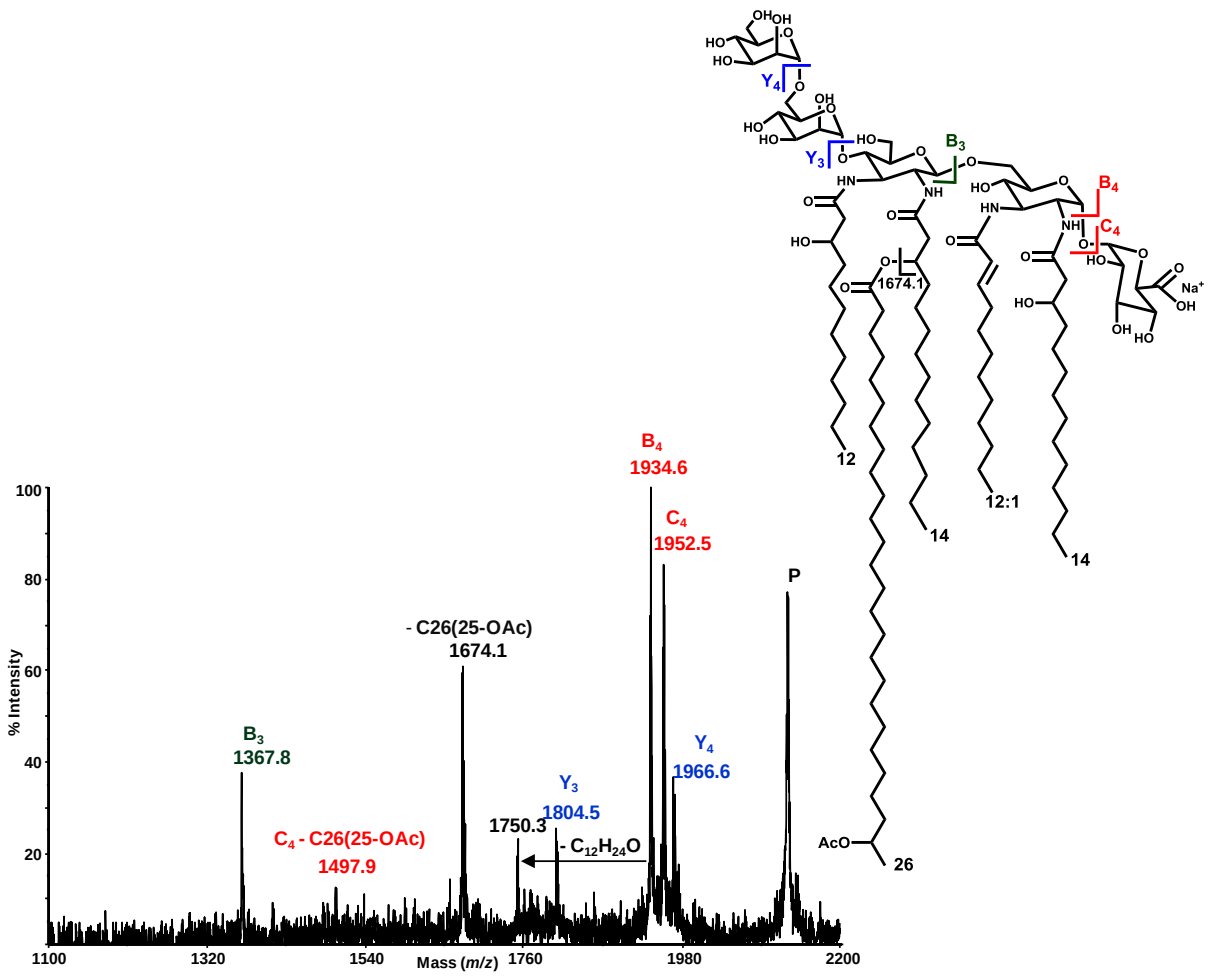

Supplementary Figure 2: MS^2 on intact penta-acylated lipid A. MALDI TOF/TOF MS^2 analysis of the penta-acylated lipid A species at *m/z* 2128.42.Loss of $C_{12}H_{24}O$ from B_4 ion is outlined in the inset of Fig. 1. P: parent ion.

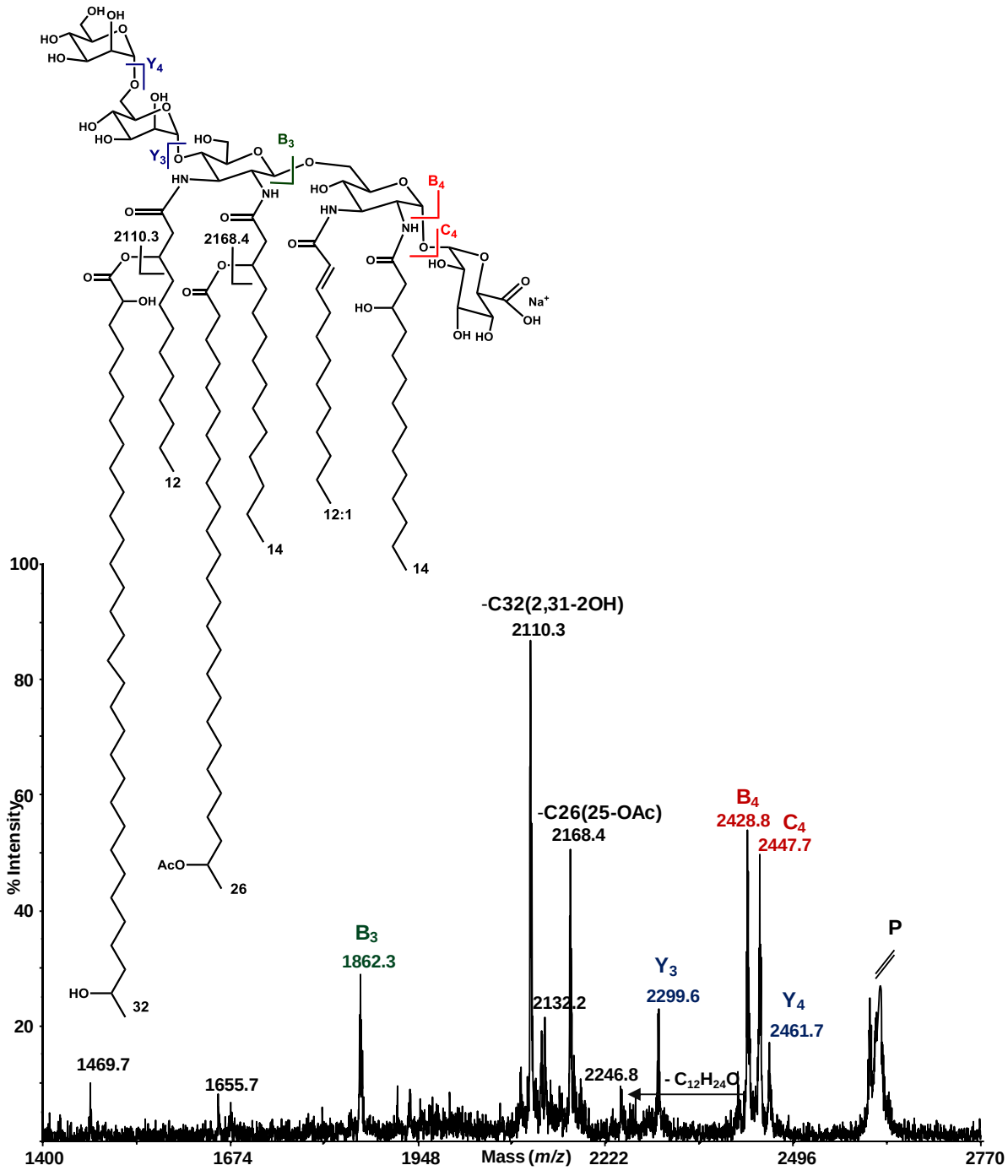

Supplementary Figure 3: MS^2 on intact hexa-acylated lipid A.MALDI TOF/TOF MS^2 analysis of the hexa-acylated lipid A species at *m/z*2622.96. Loss of $C_{12}H_{24}O$ from B_4 ion is outlined in the inset of Fig. 1. P: parent ion.

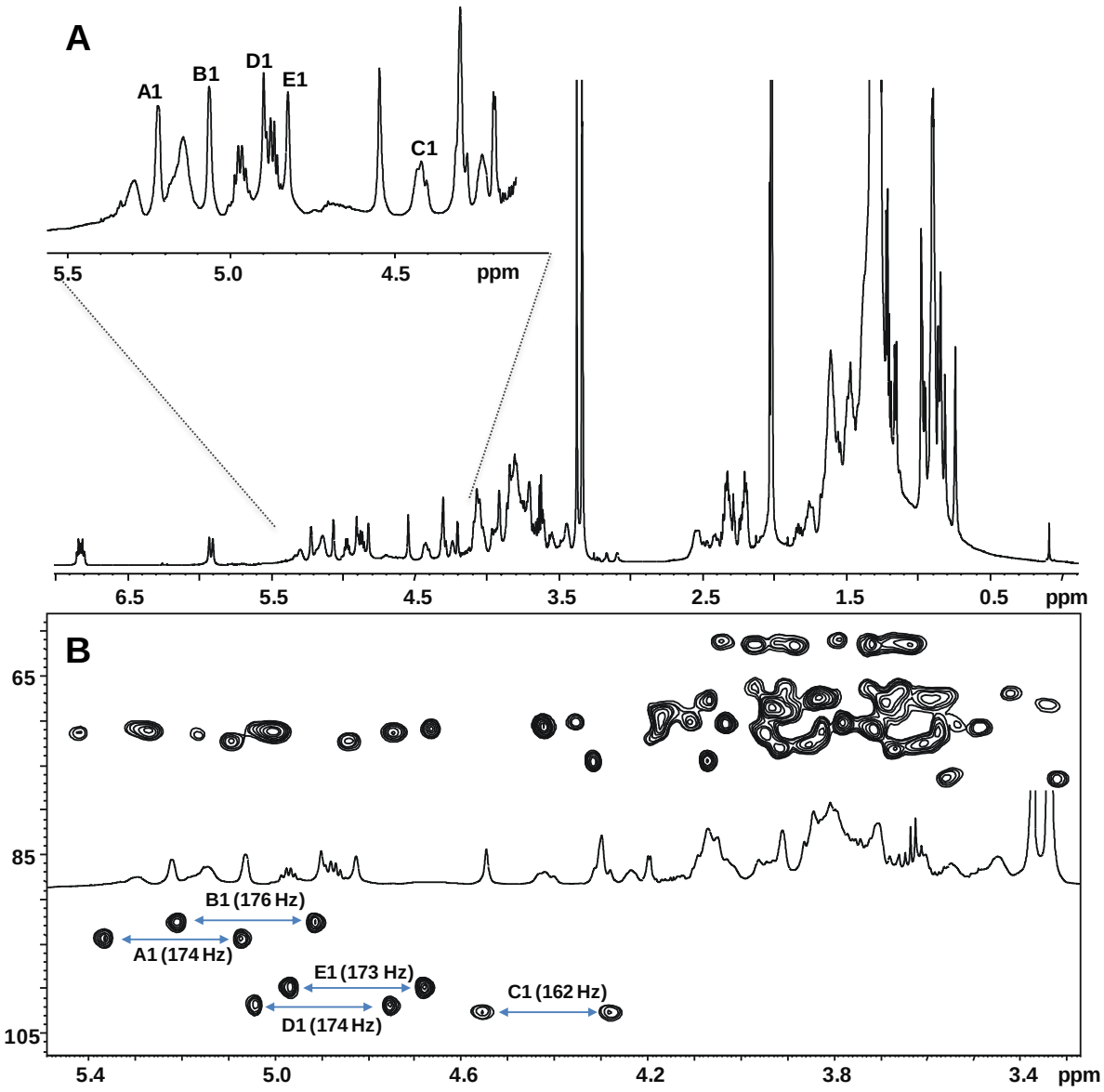

Supplementary Figure 4: NMR on intact lipid A.

a. ^{1}H NMR spectrum of the lipid A from *Bradyrhizobium*BTAi1. Anomeric signals in the inset are as attributed in Supplementary Table 2.

b. *F2-coupled* HSQC. Zoom of the anomeric region of the *F2-coupled* HSQC spectrum in which the diagnostic heteronuclearanomeric constants are shown. This experiment allowed us to define the anomeric configuration of the sugar units.

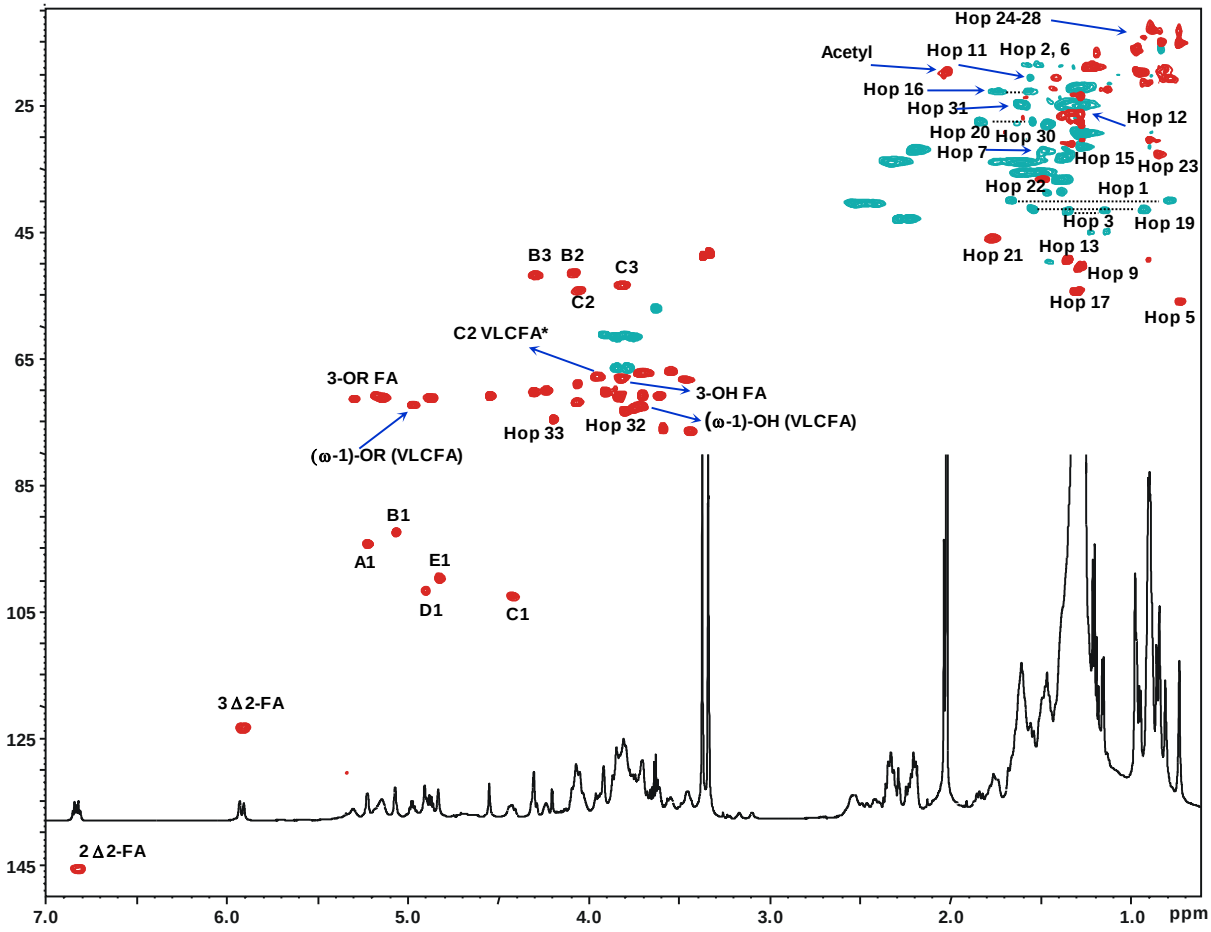

Supplementary Figure 5: HSQC NMR spectrum of *Bradyrhizobium*lipid A.
HSQC spectrum of the lipid A from *Bradyrhizobium* BTAi1. Key signals from the sugar backbone and lipid moieties are indicated. Numbering of hopanoid is as reported in Fig. 1 and Supplementary Table 2. *C2 VLCFA refers to the long chain fatty acids hydroxylated at position 2 (Supplementary Table 1-2)

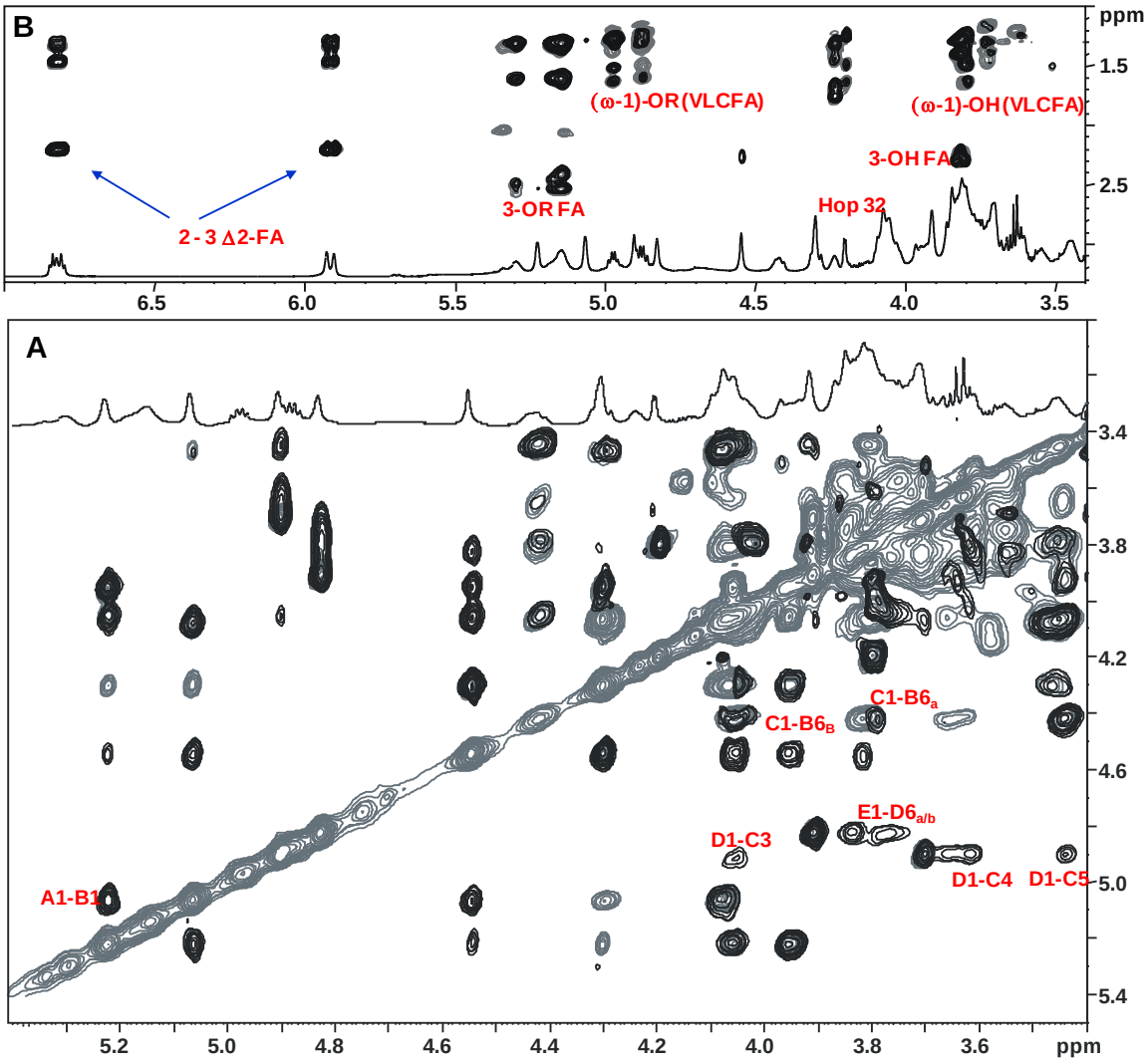

Supplementary Figure 6: Definition of the sugar skeleton and of the acylation pattern.
a. Zoom of ROESY (black) and TOCSY (grey) spectra related to the sugar resonances. The main *inter*-residual correlations used to assign, together with the HMBC spectrum, the sugar backbone, were indicated. Letters are as reported in Supplementary Table 2.
b. ROESY (black) and TOCSY (grey) spectra of the lipid A from *Bradyrhizobium*BTAi1; the differently hydroxilated lipid moieties have been indicated (Supplementary Table 2).

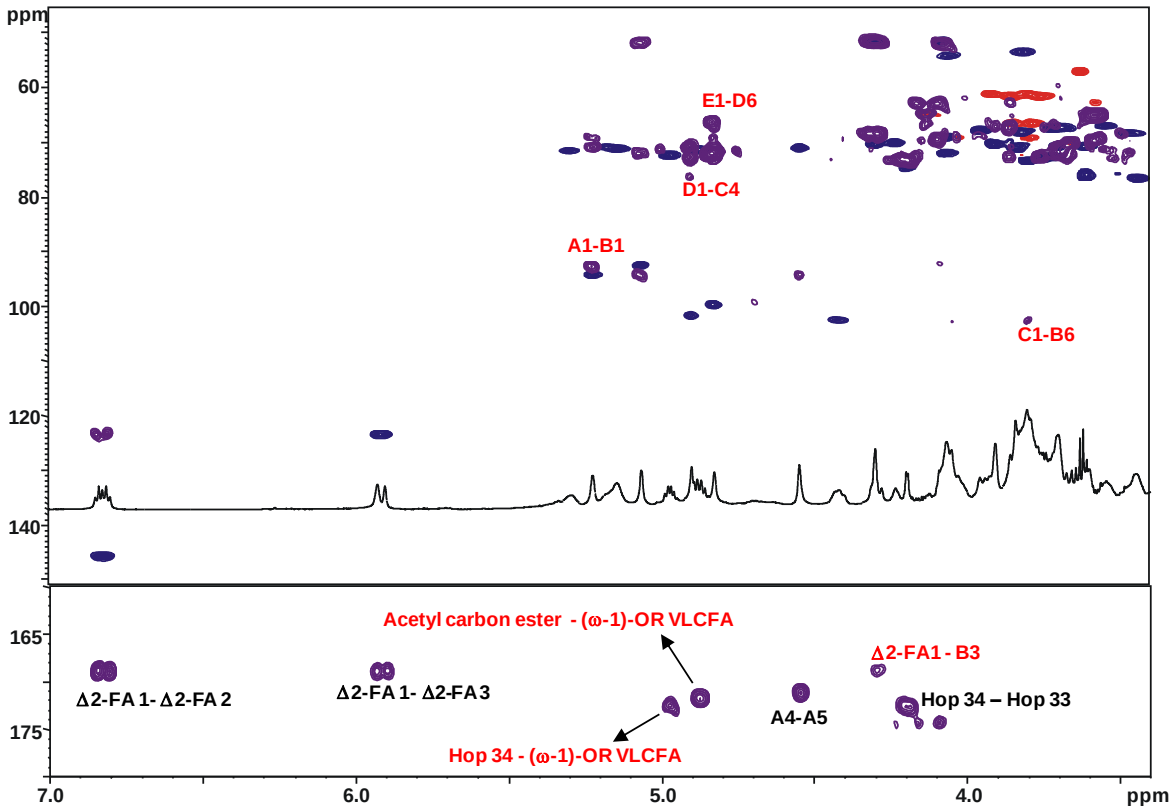

Supplementary Figure 7: HSQC and HMBC NMR spectra of *Bradyrhizobium* lipid A. HSQC (blue and red) and HMBC (violet) spectra; the key *inter*-residual long range correlations involving sugar moieties (**A-D**) and the unsaturated fatty acid (**Δ2-FA1 - B3**) are indicated in red; letters are as in Supplementary Table 2. The substitution pattern of the two *O*-acylated VLCFA were identified by the long-range correlations (red coloured) of: i) the acetyl carbon ester with the ω–1 position of a VLCFA (acetyl carbon ester - (ω-1) OR LCFA) and ii) the carbon ester at position 34 of the hopanoid with the ω–1 position of a second VLCFA (Hop 34- (ω-1) OR LCFA). Letters are as indicated in Supplementary Table2.

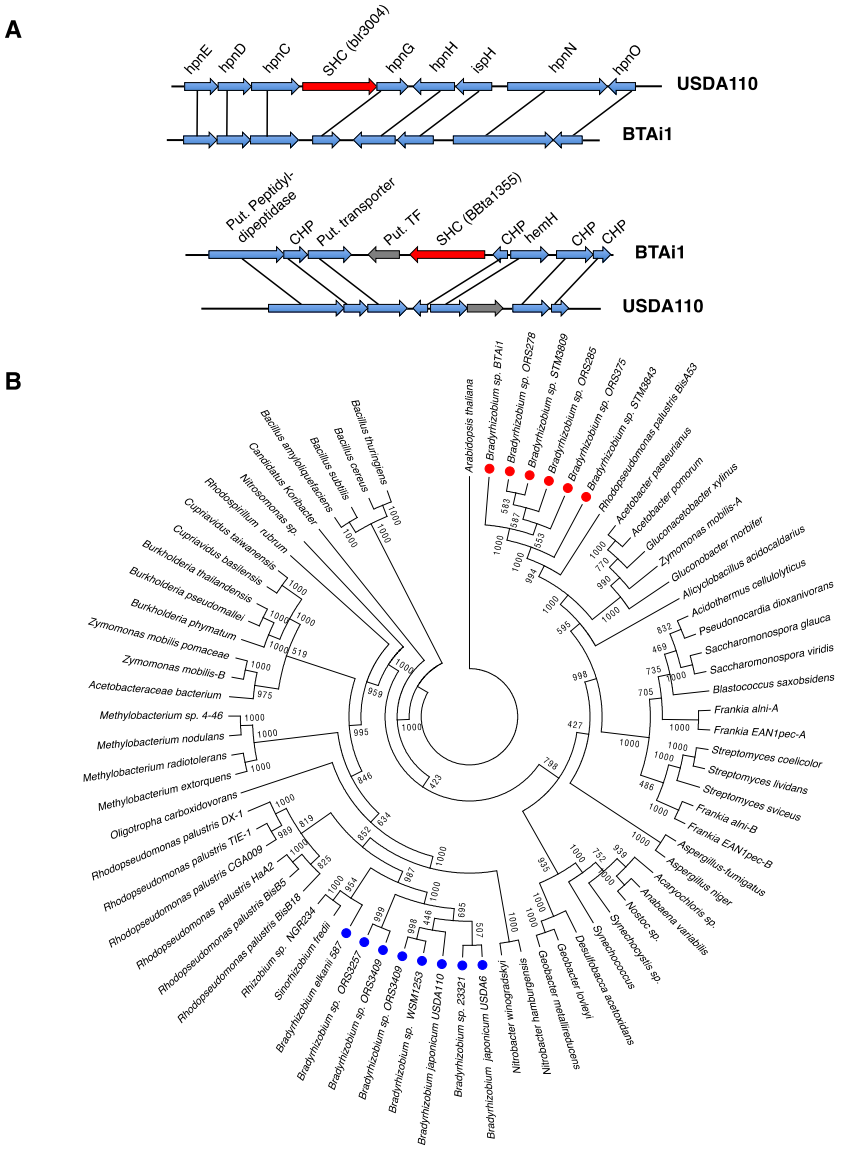

Supplementary Figure 8. Two distinct Shc identified in *Bradyrhizobium* sp. strains.
a. Genetic organization of the genes surrounding the *shc* gene in *Bradyrhizobium diazoefficiens*USDA110 and *Bradyrhizobium* sp. BTAi1. The genes annotated *hpn* were shown to be involved in hopanoid biosynthesis in *R. palustris* TIE1. In red, the *shc* gene; in blue, the genes that are found in synteny in both bacteria and in grey, genes specific to each bacteria. CHP, conserved hypothetical protein; TF, transcriptional factor.
b. Phylogenetic tree of Shc identified in various sequenced genomes. The tree was built by neighbour-joining from a matrix corrected by the Kimura-2 parameter method. Numbers at nodes are bootstrap values based on 1000 resamplings. The photosynthetic and non-photosynthetic *Bradyrhizobium* strains are marked respectively by a red and a blue circle.

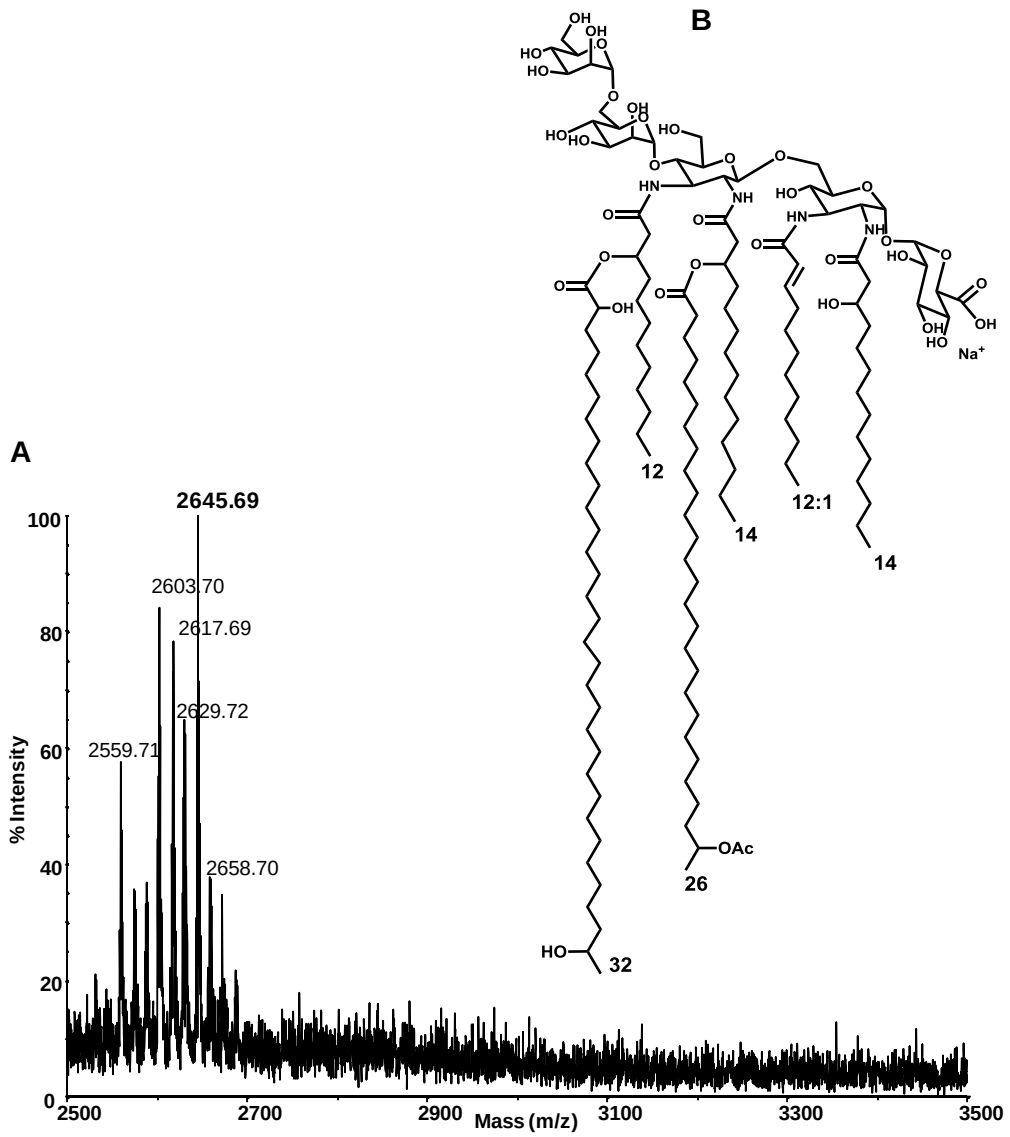

Supplementary Figure 9: Structure of the lipid A from *Bradyrhizobium*BTAi1Δshc
a. Reflectron MALDI TOF mass spectrum of the lipid A from *Bradyrhizobium*BTAi1Δ*shc* showing the complete absence of the HoLA species. All the molecular ions were detected as di-sodiated ion adducts.
b. Structure of the main lipid A species of *Bradyrhizobium*BTAi1Δ*shc* at *m/z* 2645.69.

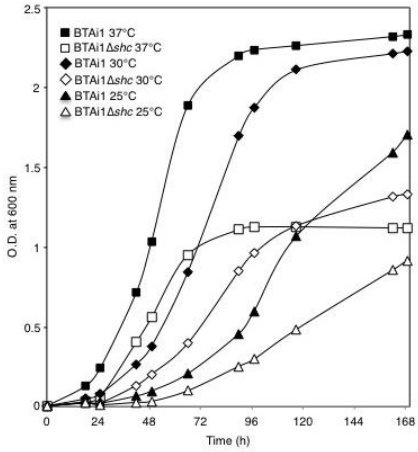

Supplementary Figure 10: Effect of the temperature on the growth.
Effect of the temperature on the growth of BTAi1 and BTAi1Δ*shc* strains cultivated in rich medium.

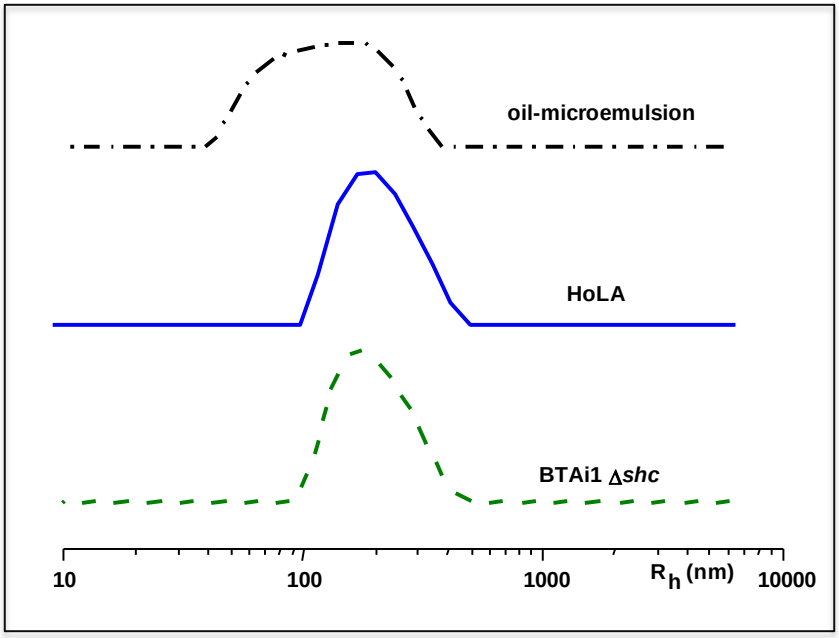

Supplementary Figure 11: DLS measurements of asymmetric liposomes.
Size distribution of emulsion and asymmetric liposomes obtained from DLS measurements performed at 90°.

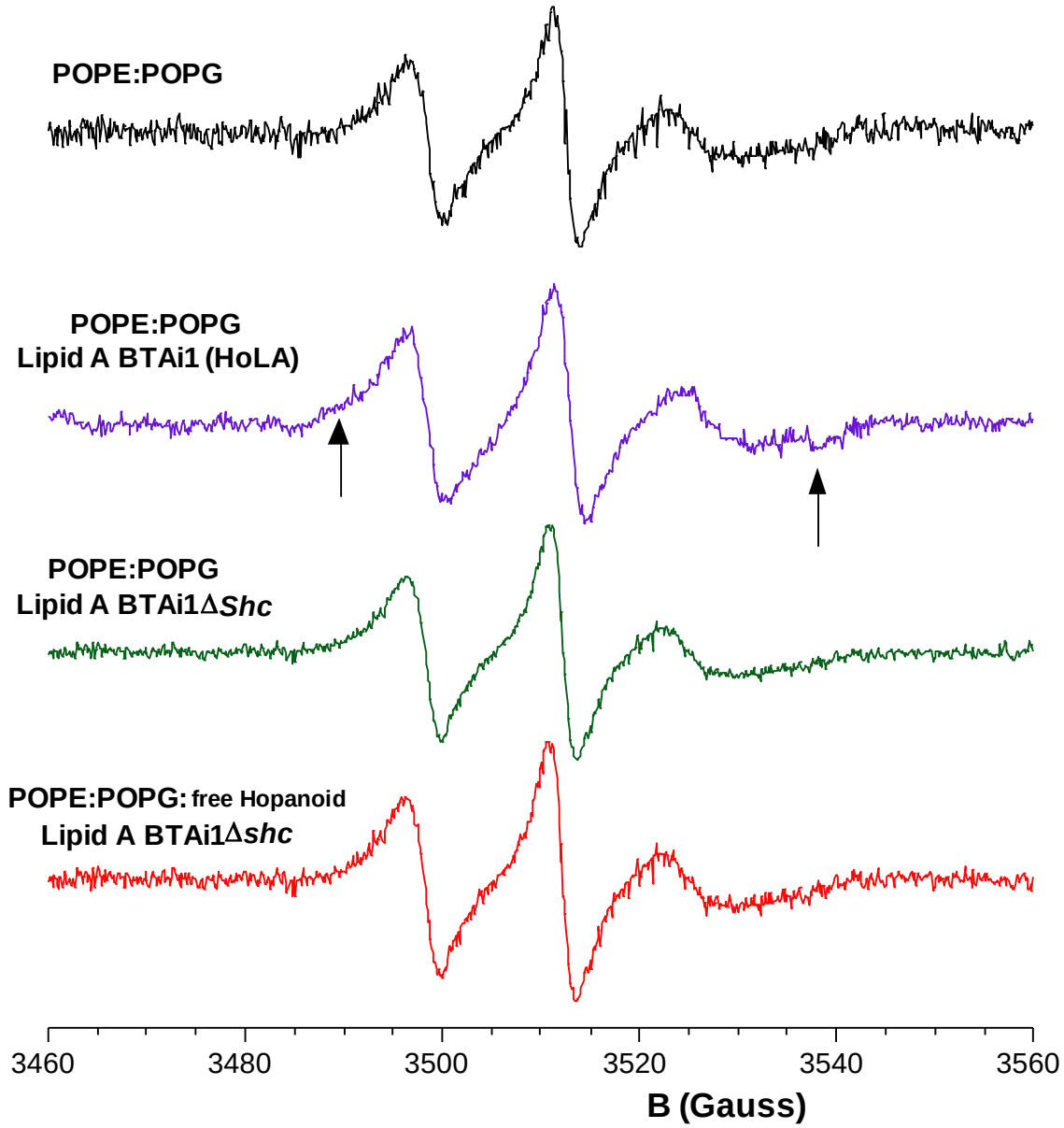

Supplementary Figure 12.EPR spectra of 14-PCSL in the inner leaflet of the asymmetric liposomes.

Components of the outer leaflet are specified in the figure. In all cases, the inner leaflet is composed by a POPE/POPG mixture. The arrows highlight the low-field shoulder and the high field minimum indicative of a second, more motionally restricted, component.

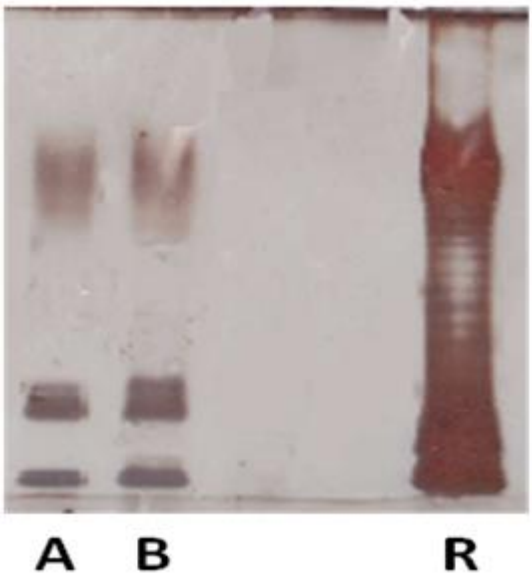

Supplementary figure 13. SDS-PAGE.

SDS PAGE of the extracted and purified LPS from *Bradyrhizobium*BTAi1 (Lane A) and *Bradyrhizobium* BTAi1Δ*shc* (Lane B); the LPS of *E. Coli* (R) was used as reference.

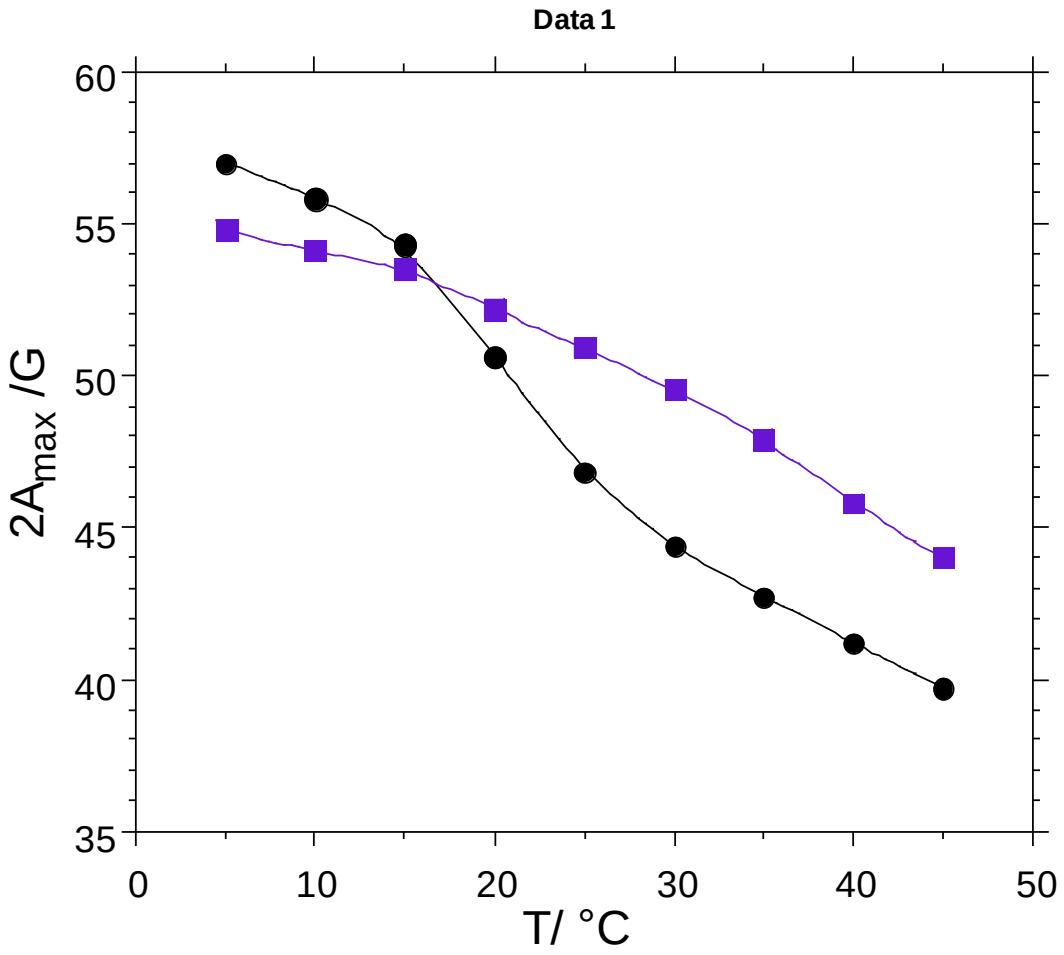

Supplementary figure 14. Outer hyperfine splitting, $2A_{max}$, of 5-PCSL in the outer leaflet of the asymmetric liposomes.

Components of the outer leaflet are POPE/POPG (black circles) or POPE/POPG/HoLA (violet squares), reported as a function of the temperature. In all cases, the inner leaflet is composed by a POPE/POPG mixture.

Supplementary Table 1: Sugar and fatty acid composition of *Bradyrhizobium* BTAi1 lipid A.

Sugar residues
GlcN3N
GalA
Man
Fatty acid residues
12:0(3-OH)
14:0(3-OH)
Δ2-12:1
12:0
26:0(25-OH)
28:0(27-OH)
30:0(29-OH)
30:0(2,29-2OH)
31:0(30-OH)
32:0(31-OH)
32:0(2,31-2OH)
33:0(2,32-2OH)
Hopanoic acid
Tetrakis-homo-hopane-32,33-diolic acid $C_{34}H_{58}O_4$

Supplementary Table 2. ^{1}H /^{13}C chemical shift values of relevant signals of lipid A from *Bradyrhizobium* BTAi1. Numbering of hopanoid signals is as reported in figure 1.

a) Sugar backbone:

Chemical shift δ (^{1}H/^{13}C)						
Unit	**1**	**2**	**3**	**4**	**5**	**6**
A	5.22	3.95	4.05	4.29	4.54	/
1–α–GalA	94.3	67.8	71.9	70.3	70.9	171.0
B	5.06	4.08	4.29	3.46	4.07	3.79/3.90
6–α–GlcN3N	92.4	51.3	51.8	68.3	71.9	69.1
C	4.41	3.8	4.07	3.65	3.44	3.91/3.80
4–β–GlcN3N	102.5	53.4	54.1	75.2	76.5	61.1
D	4.89	3.70	3.60	3.55	3.72	3.84/3.78
6–α–Man	101.8	70.7	70.7	67.0	72.5	66.5
E	4.82	3.90	3.83	3.71	3.79	3.84/3.76
t–α–Man	99.7	70.2	71.1	67.1	73.3	61.5

b) Fatty acid signals:

Fatty acid	α_1/α_2	β	γ	$(CH_2)_n$	CH_3
I–(3–OR) fatty acid	2.48/2.55	5.29	1.6	1.31	0.88
	40.63	71.32	34.08	28.6	13.0
II–(3–OR) fatty acid	2.40/2.53	5.14	1.59	1.31	0.88
	40.57	71.2	35.08	28.6	13.9
	α_1/α_2	β	γ	$(CH_2)_n$	CH_3
3–OH fatty acid	2.23/2.29	3.83	1.4	1.27	0.94
	42.9	68.1	36.6	28.6	
Acetyl group	CH_3	2.03	C=O		
		19.94	171.5		
Unsaturated fatty acid Δ2-FA	**2 Δ2-FA**	**3 Δ2-FA**			
	6.80	5.96			
	145.6	123.2			
VLCFA	**ω–2**	**ω–1**	**ω**		
verylong chain (ω-1)–OH	1.4/1.38	3.72	1.15		
	38.6	67.3	22.4		
Istverylong chain (ω-1)–OR	1.51/1.62	4.97	1.24		
Esterified by the hopanoic acid	35.6	72.3	19.1		
IIndverylong chain (ω-1)–OR	1.59/1.50	4.87	1.20		
Esterified by an acetyl group	35.5	71.3	19.0		

c) Hopanoid signals

Relevant hopanoid signals		
Position	^{1}H	^{13}C
1	0.789/1.66	39.87
2	1.50/1.38	18.6
3	1.348/1.14	41.7
4	-----	32.7
5	0.73	56.01
6	1.50/1.38	18.6
7	1.48	32.0
8	-----	41.9
9	1.28	50.37
10	-----	37.3
11	1.55	20.5
12	1.45/1.40	23.9
13	1.35	49.31
14	-----	41.7
15	1.36	33.1
16	1.55/1.73	22.67
17	1.30	54.4
18	-----	44.3
19	0.927/1.544	41.37
20	1.83/1.54	27.6
21	1.76	46.14
22	1.60	35.5
23	0.89	30.26
24	0.79	20.8
25	0.82	15.16
26	0.96	16.0
27	0.98	16.3
28	0.73	15.6
29	0.94	19.58
30	1.45	27.96
31	1.60	24.7
32	3.79	73.26
33	4.19	74.4
34	-----	172.3

Supplementary Table 3: Composition of ions present in Fig. 1c

Observed ions (*m/z*)	**MS/MS assignments**
3135.4	MNa^+
2972.7	Y_4
2959.2	C_4
2941.2	B_4
2811.1	Y_3
2757.6	$B_4 – C_{12}H_{24}O$ (see scheme in Supplementary Fig.1)
2681.0	MNa^+ - C26:0(25-OAc)
2604.8	MNa^+ - hopandiolic acid
2375.8	B_3
2111.3	MNa^+ - C32:0(2,31-2OH) - hopandiolic acid
1658.3	MNa^+ - C32:0(2,31-2OH) - hopandiolic acid - C26:0(25-OAc)

Supplementary Table 4 Values of the outer hyperfine coupling constant evaluated from the ESR spectra of 5-PCSL in outer and inner leaflet of the indicated asymmetric bilayers.

	$2A_{max}/G$ (± 0.5)
outer leaflet POPE/POPG	44.4
innerleafletPOPE/POPG	44.6
outerleafletLipidABtAi/POPE/POPG	49.5
innerleafletPOPE/POPG	52.3
outerleafletLipidA BtAi-1Shc/POPE/POPG	46.8
innerleafletPOPE/POPG	46.3
outer leaflet LipidA BtAi-1Shc/hopanoid/POPE/POPG	50.1
innerleafletPOPE/POPG	45.2

Supplementary Notes

Supplementary Note 1

Characterization of lipid A from the atomic to the supramolecular level.

Compositional analysis of the lipid A furnished the chemical constituents of the lipid A, fundamental to unveil the information provided from the other techniques. Indeed, MS gave us a picture of the molecular species composing the lipid A blend, providing important clues like the nature of heterogeneity, molecular masses, the number, the distribution and the location of lipid chains. NMR spectroscopy was used, in parallel, to unambiguously identify, at atomic resolution, lipid A constituents, for instance to define the sugar skeleton, to characterise and locate the lipids components. Once defined the structure of the lipid A, ESR and DLS techniques, performed on reconstituted bacterial membranes, were used to investigate the micro- and meso-structural properties of these systems, to monitor the characteristic of the membrane regions, such as permeability and stability, and finally to relate these supramolecular properties of the bacterial cell envelope to the molecular structure of the lipid A.

Supplementary Note 2

Isolation, purification and characterization of lipid A from *Bradyrhizobium*

Dried cells from *Bradyrhizobium*BTAi1 strain were collected and the LPS extraction was performed with hot phenol/water. The SDS-PAGE analysis of the LPS showed that BTAi1 LPS was of the smooth type, as indicated by the presence of high molecular-mass species in the upper part of the gel (Supporting Figure 13). A mild acid hydrolysis was performed on the LPS fraction to isolate the lipid A. Chemical analysis performed on the lipid A showed the presence of 6-linked and terminal mannose (Man), 6-substituted and 4-substituted 2,3-diamino-2,3-dideoxy-glucose (DAG) and terminal galacturonic acid (GalA), and, as fatty acids, 12:0(3-OH), 14:0(3-OH), Δ2-12:1, Δ2-14:1, 12:0, and the VLCFA26:0(25-OH), 28:0(27-OH), 30:0(29-OH), 30:0(2,29-2OH), 31:0(30-OH), 32:0(31-OH) (Supplementary Table 1). Usually, the Δ2-unsaturated fatty acids represent artefacts originating from β-elimination of 3-OH fatty acids, occurring during fatty acid analysis, however, NMR and MS data confirmed that Δ2-12:1 was present as component of the lipid A (see below). In addition,

Lipid A GC-MS analysis also showed the presence of hopanoids. In particular, GC-MS data showed the presence of hopanediolic acid (Fig. 1a).

Supplementary Note 3

MALDI TOF MS and MS/MS analysis of lipid A.

MS and MS/MS analysis on the *O*-deacylated lipid A were performed; the main molecular ion [M+Na^+] at *m/z*1691.76,present in the MALDI TOF spectrum (data not shown), was found consistent with a tetra-acylated oligosaccharide backbone (two DAG, two Man, one GalA) connected with two 14:0(3-OH), one 12:0(3-OH) and one unsaturated 12:1. The detailed structure of this species was accurately defined by MALDI TOF/TOF MS^2 analysis (Supplementary Fig. 1). All the fragment ions accounting for the cleavage of the glycosidic bonds (as sketched in the *O*-deacylated lipid A structure also present in Supplementary Fig. 1, pointed to a saccharide sequence on the DAG backbone in fully accordance with the NMR data. Actually, Y_4 (*m/z*1529.9) and Y_3 ions (*m/z*1367.8) corresponded to the loss of one and two Man residues respectively from the non-reducing oligosaccharide end. The fragmentation spectrum also showed a very informative peak at *m/z*931.5identified as a B_3 ion generated from the rupture of the glycosidic linkage between the two aminosugars and consisting in two Man and one DAG N-substituted by a 14:0(3-OH) and a 12:0(3-OH) acyl moiety. A subsequent rearrangement of B_3 ion, promoted by the free 3-OH group on the14:0 (as described in the inset in Supplementary Fig. 1), resulted in the loss of 184mass units ($C_{12}H_{24}O$), giving the ion at *m/z*747.2 (Supplementary Fig.1). This fragmentation was very helpful to establish that the primary acylated 14:0(3-OH) is sitting at position 2 of the distal DAG. In addition, fragments at *m/z*1515.9, 1497.9 and 1313.8were informative of the location of primary acyl chains on the proximal DAG residue. In detail, the loss of the reducing terminal GalA gave B- and C-type ions as very abundant species at *m/z* 1515.9 (C_4) and 1497.9(B_4). Further fragmentation of B_4, analogously to B_3 ion, originated the peak at *m/z*1313.8(loss of $C_{12}H_{24}O$, see Supplementary Fig. 1 inset). All these results proved that the primary 14:0(3-OH) is located at position 2 of the DAG and, as a consequence, the unsaturated acyl moiety 12:1 is *N*-linked at position 3.

The positive ion MALDI spectrum performed on the intact lipid A (Fig. 1b) exhibited a heterogeneous mixture of ion peaks (present as Na^+ adducts) belonging to three families of lipid A species which differed in the acylation pattern at the saccharide skeleton; for each series, whose major components were found at *m/z*2128.42, 2594.93 and 3107.34, the mass differences between neighbouring ions were due to the different lengths and/or substitution

pattern of the ester-linked acyl chains (Supplementary Table 1). The lowest molecular mass peak at *m/z*2128.42was found compatible with a penta-acylated species with two 14:0(3-OH), one 12:0(3-OH), one 12:1 and one 26:0(25-OAc); it is worth to note that no additional peaks were observed in the mass-range nearby the penta-acyl lipid A moiety, thus indicating that no heterogeneity, neither in the length nor in the substitution pattern, is due to the ester linked 26:0(25-OAc).The positive ion MS/MS spectrum of this parent ion (*m/z*2128.42) reported in Supplementary Fig.2, showed, besides the ion series generated from the cleavage of the glycosidic linkages (i.e. Y_4 at *m/z*1966.6, C_4 at *m/z*1952.5, B_4 at *m/z*1934.6, and Y_3 at *m/z*1804.5) also a significant ion peak at *m/z*1674.1, corresponding to a tetra-acylated fragment devoid of the VLCFA 26:0(25-OAc). Moreover, the overall fragmentation pattern allowed to ascertaining the exact position of this secondary *O*-substitution: peaks at *m/z*1934.6 and 1367.8were both referred to B-type ions (B_4 and B_3 respectively) originated from the glycosidic linkage cleavages *via* β-elimination. In particular B_3 ion at *m/z*1367.8, consistent with a tri-acylated lipid A fragment having 14:0(3-OH) and 12:0(3-OH) as primary and 26:0(25-OAc) as secondary acyl substituents, provided a clear evidence that this latter moiety was bound to the non-reducing DAG residue. Since, unlike the B_4 ion flanking peak at *m/z* 1750.3due to the meaningful loss of 184mass units ($C_{12}H_{24}O$), no additional signal was found in the mass-range below B_3, it could be reasonably inferred that the 3-OH substitution on 14:0 by the secondary acyl chain prevents the molecular rearrangement leading to that fragmentation, thus suggesting that the VLCFA 26:0(25-OAc) was located on the 14:0(3-OH) occurring at position 2 of the distal DAG.

The MS/MS analysis on the parent ion at *m/z*2622.96(Supplementary Fig.3) showed this species corresponding to a hexa-acylated lipid A sharing with the penta-acylated ion at *m/z* 2128.42the same structure plus an additional secondary VLCFA recognized as 32:0(2,31-2OH). In this case, B_3 ion found at *m/z*1862.3, was consistent with the following composition: one residue of GlcN3N, two residues of Man, one 14:0(3-OH), 12:0(3-OH), 26:0(25-OAc), 32:0(2,31-2OH), allowing us to disclose a peculiar lipid A architecture characterized by an asymmetric distribution of the acyl chains with respect to the DAG disaccharide backbone of the hexa-acylated species (4+2 arrangement). To sum up, the hexa-acylated family of lipid A originated from acyl-substitution at position 3 of the primary acyl chain located on the non-reducing DAG; both MS and MS/MS data suggested that the heterogeneity of this secondary fatty acids could be ascribed to mono and/or bis-hydroxylated 30:0, 31:0 and 32:0.

The third lipid A family was shifted to higher molecular mass by Δ*m/z* 512.4, the mass difference corresponding to a hepta-acylated structure carrying an additional hopanoid residue

(molecular formula $C_{34}H_{56}O_3$). The ion pattern in the MS/MS spectrum (Fig. 1c), following a fragmentation scheme similar to that previous observed, allowed us to draw the complete structure of the lipid A from *Bradyrhizobium sp.* BTAi1: the ion peak at *m/z* 2604.8corresponded to the hexa-acylated lipid A fragment lacking the residue of hopanoid (loss of 530 mass units, Fig. 1c) while the ion at *m/z*2111.3was the result of the loss of the whole *O*-acyloxyacyl group composed of the hopanoid residue linked to 32:0(2,31 2-OH). This finding indicated the hopanoid moiety as a tertiary substitution, located, as evinced from NMR analysis below, at the ω-1 position of the long chain fatty acid.

Supplementary Note 4

NMR spectroscopy of lipid A

For the NMR characterization, lipid A was dissolved in $CDCl_3/CD_3OD$ (^{1}H NMR spectrum in Supplementary Fig. 4a). A combination of homo- and heteronuclear 2D NMR experiment (DQF-COSY, TOCSY, TROESY, NOESY,^{1}H-^{13}C HSQC, ^{1}H-^{13}C HMBC, $^1J_{CH}$ HSQC) was executed in order to assign all the spin systems and to define the saccharidic sequence (Supplementary Table 2). The anomeric configuration of each monosaccharide unit was assigned on the basis of $^1J_{C1,H1}$constants derived by *F2-coupled* HSQC (Supplementary Fig. 4b) and confirmed by the *intra*-residual NOE contacts. In the HSQC spectrum (Supplementary Fig.5) five cross peaks were located in the anomeric region, four signals, between 50 and 55 ppm, were attributable to nitrogen-bearing carbons, while in the region from 60 to 78 ppm resonated ring carbons as well as hydroxylated acyl chains and hopanoid moieties; other signals were clearly visible in the aliphatic and olephinic region. Coupling constants and chemical shift values were in agreement with the presence of two DAG residues, two residues of Man*p* and one of Gal*p*A, all present in $^4C_1$ chair conformation. In detail, the anomeric protons at 5.06 ppm (**B**) and 4.41 ppm (**C**) were respectively identified as α and β residues; their anomeric configuration was determined by the $^1J_{C1,H1}$ constants (Supplementary Fig. 4b and Supplementary Table 2) derived from *F2*-coupled HSQC measurements, and confirmed by the *intra*-residual NOE contacts observed in the ROESY spectrum (Supplementary Fig. 6a). Spin system **B** presented a $^1J_{C1,H1}$ value of 176 Hz and an *intra*-residual NOE contact of **B**-1 only with **B**-2, confirming the α-configuration. Spin system **C,** instead, presented a $^1J_{C1,H1}$ value of 162 Hz and NOE correlations of **C**-1 with **C**-2, **C**-3 and **C**-5, typical for a β-configuration. The carbon chemical shifts of **B**-2/**B**-3 (51.3/51.78 ppm) and **C**-2/**C**-3 (53.48/54.17 ppm) corresponded to *N*-linked carbons, in accordance with

the presence of DAG. The downfield shifts of the proton resonances of H-2 and H-3 of residues **B** and **C** were diagnostic for their *N*-acylation. The carbon resonance of **B**-6 (69.19 ppm) was evidently shifted downfield suggesting a glycosylation at this position. The anomeric proton of residue **C** presented a strong NOE correlation with **B**-6 suggesting that the two GlcN3N were β–(1→6)-linked, as confirmed by the corresponding long-range correlation.

Spin system **A** (5.22, 94.3 ppm) was assigned to an α-Gal*p*A residue. The $^{3}J_{H3,H4}$and $^{3}J_{H4,H5}$ values (below 1 Hz) were in accordance with a *galacto*-configuration. The α-configuration was inferred by the heteronuclear$^{1}J_{C1,H1}$ value of 174 Hz, and confirmed by H-1/C-1 chemical shifts and by the *intra*-residual NOE contact of H-1 with H-2. The ring carbon resonances of **A** were not shifted downfield suggesting that this residue was terminal, in accordance with methylation analysis. The strong NOE contact between the anomeric protons of residues **A** and **B** and the long-range correlations between these two positions were diagnostic for their trehalose-like α,α–(1→1) linkage.

Residues **D** and **E** were α-Man*p* units. The *manno*-configuration was assigned by $^{3}J_{H1\text{-}H2}$ and$^{3}J_{H2\text{-}H3}$ values (below 3 Hz), whereas the anomeric configuration was established by the $^{1}J_{C1,H1}$ value and the *intra*-residual NOE contact of H-1 with H-2. The downfield shift of C-6 from residue **D** together with the strong NOE contact between **E**1 and **D**6’/**D**6” and the corresponding long range correlation (Supplementary Figs. 6a and 7, Supplementary Table 2) indicated that they were bound trough anα-(1→6)-linkage. Furthermore, the anomeric carbon of residue **D** presented a strong HMBC signal with H-4 from residue **C** (Supplementary Fig. 7) suggesting that the Man **D** was α-(1→4)-linked to the distal β-DAG unit.

In summary, all the NMR fully supported the existence of a pentasaccharide backbone formed by a skeleton of β–(1→6) linked DAG substituted by an α-GalA in trehalose-like α,α–(1→1) linkage on the vicinal DAG and by an α-(1→6) Man disaccharide α-(1→4)-linked to the distal β-DAG unit:

E **D** **C** **B** **A**

Man*p*-α-(1→6)-Man*p*-α-(1→4)-Glc*p*N3N–β–(1→6)–Glc*p*N3N-α-(1→1)-α-Gal*p*A

A thorough analysis of the NMR spectra allowed us to further detail the spectroscopic characterization of the lipid A from *Bradyrhizobium* BTAi1. Several spin systems were

attributed to the acyl moieties. In the HSQC spectrum (Supplementary Fig. 5), the cross peaks at 3.83/68.1 ppm corresponded to H3/C3 of primary 14:0(3-OH) and 12:0(3-OH) moieties while the downfield signals at 5.29/71.32 ppm and 5.14/71.2 ppm were assigned to *O*-acylated H3/C3 of the same residues (Supplementary Figs. 6b and 7). The chemical shifts for α,β and γ atoms of 3-OH fatty acids are listed in Supplementary Table 2. In addition, two low field signals at 6.80/145.6 and 5.96/123.2 ppm and both correlated to an acyl carbon at 169 ppm were attributed to the double bond of a α,β unsaturated fatty acid (Δ2-FA, Supplementary Table 2, Supplementary Figs. 5-7). Interestingly, this unsaturated acyl moiety was clearly located at position 3 of the vicinal DAG, residue **B**, as evident from the long range correlation in the HMBC spectrum (Supplementary Fig. 7) between H3 **B** and C1 of Δ2-FA, as was further confirmed by the analysis of the MS spectra (see above).

The proton signal at 3.72 ppm correlated, in HSQC spectrum, to a carbon signal resonating at 67.3 ppm, was identified as the ω-1 methine of the long chain fatty acids, in turn connected to a methyl group at 1.15 ppm and to the ω-2 methylene protons at 1.4/1.38 ppm. Furthermore, NMR data also showed the correlation of a methyne group at 4.23/70.1 ppm with carbonyl and methylene groups (Supplementary table 2, Supplementary Fig. 6b), attributable to long chain fatty acids partially hydroxylated at position 2, in accordance to the chemical analysis (Supplementary Table 2). Analysis of the NMR spectra allowed to identify and locate the triterpenoid moiety constituting the hopanoid skeleton, in full accordance with the previously discussed GC-MS data. Particularly significant were the methyl signals resonating in the region between 0.6-1.0 ppm typical of the angular methyl constituents of the terpenoid moiety. The hopanoid resonances were attributed also on the basis of previously published data[1-3].Two further ω-1 methine groups (4.97/4.87 and 72.3/71.3 ppm respectively), were identified as *O*-acylated long chain fatty acid. The nature of their *O*-substitution was established as follow. The long range correlation present in the HMBC spectrum (Supplementary Table 2, Supplementary Fig. 7) between the ester carbon at 171.7 ppm, the ω−1 group of the LCFA at 4.87 ppm and the methyl acetyl group at 2.02 ppm was a proof of the *O*-acetylation of this lipid moiety. Furthermore, the long range correlation allowed to locate the hopanoid moiety on the second acylated LCFA. Actually, in the HMBC spectrum, the ester carbon at position 34 of the hopanoid moiety, Hop34, at 172.3 ppm, showed an *intra*-residual long range correlation with position 33 (Hop33) at 4.19 ppm and an *inter*-residual long range correlation with positions ω−1 of the LCFA at 4.97 pm, demonstrating the chemical linkage between the two moieties. Therefore, the hopanoid was attached, by an ester

linkage, at the ω−1 hydroxyl group of the long chain acyl moiety. In conclusion, the two VLCFA were esterified respectively by an acetyl group and a hopanoid residue.

Supplementary Note 5

Supramolecular arrangement of *Bradyrhizobium* cell envelope: role of lipid A and hopanoids in the stability of the outer membrane

In order to investigate by ESR the microstructure of membranes from*Bradyrhizobium*BTAi1 and BTAI1Δ*shc* mutant, the respective lipid A (Fig. 2 and Supplementary Fig. 9b) were included in the formulation of biomimetic liposomes prepared *in vitro*. Realistic models of the outer membrane of Gram-negative bacteria must incorporate lipid asymmetry, with all the LPS molecules in the outer leaflet of the lipid bilayer, the inner one being constituted by glycerophospholipids. For this reason typical methods for liposome preparation (e.g., sonication, extrusion, electroformation) have to be discharged. Different methods to prepare asymmetric liposomes have been presented in the literature. Partial asymmetry can be achieved by altering the distribution of specific phospholipids in pre-formed symmetric liposomes using external stimuli (e.g. pH gradients, osmotic pressure, or molecules that promote lipid redistribution).

However, the chemical constraints of these methods severely limit their applicability to our systems. In this work, we have adopted a protocol for asymmetric liposome preparation based on the assembly of two independently-prepared lipid monolayers[4]. It is the first time this method is used for liposomes including LPS and some modifications to the original protocol were required, as detailed in the method section (Fig. 7a and Supplementary Fig. 11). To determine the different physical properties of the two lipid leaflets, as derived from the different lipid composition, ESR spectra of spin-labelled lipids, purposely included in the liposome formulation, were registered[5-6].

The 5-PCSL spectra obtained for the lipid bilayers considered in this work at 30 °C are shown in Fig. 7b. As detailed in the experimental section, for each bilayer the molecular probe was inserted either in the outer leaflet or in the inner one.5-PCSL is a spin-labeled lipid bearing the nitroxide reporter group attached to the acyl chain in position 5, i.e. relatively close to the hydrophilic headgroup. Thus, it monitors the local structuring and dynamics of the lipid tails just underneath the polar interface between the membrane and the aqueous medium. The 5-PCSL ESR spectrum has been found to be highly sensitive to pseudo-phase transitions of lipid membranes from a disordered to an ordered state. In the disordered liquid crystalline state,

also named L_α, the carbon bonds in the lipid acyl chains presents both trans and gauche conformations rapidly interconverting, thus forming an hydrophobic core of the membrane closely resembling a liquid "oil". In the ordered states the acyl chains preferentially present all-trans conformations and tend to align in the same direction, thus forming a viscous and molecularly ordered hydrophobic core. Molecularly ordered membranes can be induced by a lowering of the temperature (solid or gel state, also named L_β) or by the presence of a guest molecule which "orders" the adjacent lipid chains (ordered liquid crystalline state, L_o). L_β and L_o membranes present the same short-range order constrains, only differing in long-range translation capabilities of the lipids along the bilayer, which is higher for the L_o membranes. From a macroscopic and functional viewpoint, both L_β and L_o membranes are more rigid and less permeable than L_α ones. Symmetric lipid bilayers formed by LPS usually present a transition from L_β to L_α with increasing the temperature above 20-25 °C. The presence of polycyclic compounds such as hopanoids, stabilizes an ordered L_o state even at higher temperature, thus improving the membrane strength and rigidity. In this respect, hopanoids serve the same function of sterols (e.g. cholesterol) in eukaryotes.

To the best of our knowledge, we have here reported the first investigation on the liquid crystalline state of asymmetric bilayers presenting one of the lipid leaflets (the outer one) predominantly composed by LPS. Here, we start with analyzing, as reference system, symmetric POPE/POPG bilayers. Inspection of Fig. 7b shows that 5-PCSL molecules present similar spectra when inserted in the outer or in the inner leaflet of such bilayers, thus confirming the symmetry of the membrane. The spectrum lineshape shows a marked anisotropy, as expected for spin-labels whose motions are significantly restricted by the neighboring acyl chains. The extent of this anisotropic behavior can be quantitatively estimated by measuring the outer hyperfine coupling constant, $2A_{max}$, defined as the distance, in Gauss, between the low-field maximum and the high-field minimum. In lipid bilayers, $2A_{max}$ is an index of the local ordering of the lipid chains and, consequently, of the membrane fluidity. The $2A_{max}$ values obtained by the analysis of all the spectra shown in Fig. 7b are collected in Supplementary Table 4, whose inspection confirms that the leaflet of symmetric POPE/POPG bilayers present the same behavior. Quantitatively, the observed $2A_{max}$ values indicated that the membrane was in the fluid L_α state[7].

As second lipid system, we considered asymmetric bilayers including HoLA in the outer leaflet formulation. The 5-PCSL spectra appear significantly affected by this insertion, showing a larger anisotropic lineshape for both bilayer leaflets, as also confirmed by the

increased $2A_{max}$ values reported in Supplementary Table 4. This evidence indicated that HoLA insertion in the outer leaflet caused a lower fluidity of the whole membrane, evocative of its mechanical strengthening. Unexpectedly, the inner leaflet was even more affected by HoLA presence than the outer leaflet, in which this lipid A had been positioned. This demonstrates that the long acyl chains of the lipid A from *Bradyrhizobium* BTAi1 passed through the membrane, so that the terminal hopanoid appendages were positioned in the inner leaflet (see the sketch in Fig. 7b). The result of this lipid arrangement is twofold: (i.) both leaflets were much more ordered and (ii.) the leaflets were tightly linked among them, the long acyl chains acting as a "tightrope" between the two membrane interfaces.

As third lipid system, we considered asymmetric lipid bilayers including lipid A from BTAI1Δ*shc* mutant in the outer leaflet formulation. In this case, the 5-PCSL spectra showed that the outer leaflet was less fluid than the inner one (see also Supplementary Table 4). Furthermore, the whole bilayer was less ordered that that in which the HoLA was present. This evidence indicated that the hopanoid moiety linked at a terminus of one acyl chain was essential to drive its insertion among the lipid chains of the opposite leaflet.

Finally, we considered a membrane whose outer leaflet contained the lipid A from BTAI1Δ*shc* mutant and hopanoid extracts. The 5-PCSL spectra and the $2A_{max}$ values showed that only the outer leaflet was affected by the hopanoid ordering effect, while the inner one remained almost unperturbed. It could be concluded that the long acyl chain was necessary to drive the hopanoid moiety to the inner leaflet, otherwise it tend to reside among the lipid A chains of the outer one. It is to be observed that lipid bilayers in which the outer and inner leaflet present a very different ordering, like the last we have considered, are usually unstable.

A further confirmation of our interpretation of 5-PCSL spectra comes from the spectra of 14-PCSL spectra inserted in the inner leaflet of the analyzed lipid systems, reported in Figure S12. As opposed to the clearly defined axially anisotropic spectra that are obtained for 5-PCSL, a narrower, three-line, quasi-isotropic spectrum is generally obtained for 14-PCSL, which bears the nitroxide reporter group attached to the acyl chain in position 14, i.e. close to the terminal methyl region of the chain. This flexibility gradient in segmental chain mobility, quantitatively confirmed by the $2A_{max}$ values reported in Supplementary Table 4, is a characteristic hallmark of the liquid-crystalline state of phospholipid bilayers. Perusal of the figure shows that the spectrum in bilayers including HoLA in the outer leaflet presents a second component, which is particularly evident in the low-field shoulder and high-field minimum highlighted by the arrows. This is clear evidence of a more ordered arrangement of the motionally restricted lipid tails, an effect of the long acyl chain insertion through both

lipid leaflets, the terminal hopanoid appendage acting as an anchor to the opposite bilayer surface (see the sketch in Fig. 7b).

Finally, the spectra of 5-PCSL inserted in the outer leaflet of either POPE/POPG symmetric bilayers or POPE/POPG/HoLA asymmetric bilayers were registered as a function of the temperature. The trends of the $2A_{max}$ values are shown in Supplementary Figure 14. In the case of POPE/POPG liposomes, a broad inflection is observed between 15 and 25 °C, corresponding to the increase in lipid chain mobility on the transition from the gel to the fluid phase. For POPE/POPG/HoLA asymmetric bilayers a much smoother decrease is observed, with no evident transition. Interestingly, HoLA increases the bilayer fluidity at low temperature, while causes its stiffening above ~15 °C.

In conclusion, all our results highlight that the molecular structure of HoLA is optimally suited to induce a high ordering of the bacterial asymmetric outer membrane, which results in its mechanical strengthening and stabilization.

Supplementary References

1. Costantino, V., Della Sala, G., Mangoni, A., Perinu, C. & Teta R. Blurring the BoundarybetweenBio- and Geohopanoids: Plakohopanoid, a C32 Biohopanoid Ester from Plakortiscf. lita, *Eur. J.Org. Chem.*, **2012**, 5171-5176 (2012).

2. Nytoft, H.P., Lutnæs, B.F. &Johansen, J.E. 28-Nor-spergulanes, a novelseries of rearrangedhopanes, *Organic Geochemistry***37**, 772–786 (2003).

3. Choma, A. &Komaniecka, I. Straight and branched (ω-1)-hydroxylatedvery long chainfattyacids are components of *Bradyrhizobium*lipid A. *Acta Biochim Pol*.**58**, 51-8 (2011).

4. Pautot, S., Frisken, B. J.&Weitz, D. A. Engineering asymmetric vesicles. *Proc. Natl. Acad. Sci. USA.***100**, 10718-10721 (2003).

5. D'Errico, G. *et al*.Mesoscopic and microstructural characterization of liposomesformed by the lipooligosaccharide from *Salmonella minnesota* strain 595 (Re mutant). *Phys. Chem.Chem. Phys.*, **11**, 2314-2322 (2009).

6. D'Errico, G. et al. Characterization of liposomesformed by lipopolysaccharides from *Burkholderia cenocepacia*, *Burkholderia multivorans* and *Agrobacterium tumefaciens*: from the molecularstructure to the aggregate architecture. *Phys. Chem. Chem. Phys.***12**, 13574–13585 (2010).

7. D'Errico, G., D'Ursi, A. M. &Marsh, D. Interaction of a peptide derived from glycoprotein gp36 of Feline Immunodeficiency Virus and itslipoylatedanalogue with phospholipidmembranes).*Biochemistry*, **47**, 5317-5327 (2008).